Green Chemistry

Accepted Manuscript

ROYAL SOCIETY OF CHEMISTRY

rsc.li/green-chem

View Article Online
DOI: 10.1039/C8GC01522H

Journal Name

ARTICLE

Palladium nanodendrites uniformly deposited on the surface of polymers as an efficient and recyclable catalyst for direct drug modification *via Z*-selective semihydrogenation of alkynes†

Received 00th January 20xx,
Accepted 00th January 20xx

DOI: 10.1039/x0xx00000x

www.rsc.org/

José García-Calvo,[a] Patricia Calvo-Gredilla,[a] Saúl Vallejos,[a] José Miguel García,[a] José Vicente Cuevas-Vicario,[a] Gabriel García-Herbosa,[a] Manuel Avella,[b] Tomás Torroba[a,*]

The preparation of new monodisperse polycrystalline palladium nanoparticles uniformly distributed on the surface of polymers, by simply adding a palladium(II) solution in water to the polymers, is described. The polymer supported palladium nanoparticles material was used as an efficient portable and reusable catalyst for the stereoselective semihydrogenation reaction of internal alkynes to (*Z*)-alkenes in green solvents.

Introduction

The preparation of solid-supported palladium nanoparticles of well-defined shape and size is an important goal for the achievement of new palladium nanomaterials with clear-cut properties for innovative green catalytic processes.[1] Shape controlled palladium nanoparticles need careful nucleation and growth conditions,[2] specially in aqueous solutions,[3] and manipulation of kinetic parameters.[4] The presence of an organic stabilizer system permits control over the reaction kinetics and hence, the shape of the nanostructures.[5] Additives usually help for the generation of monodisperse, water-soluble palladium nanoparticles of controlled size, such as peptides,[6] often serving as reducing and capping agents, for instance hexacarbonylmetals,[7,8] acids, amines and CO[9] or EDTA.[10] Careful guiding of the reaction kinetics with additives such as polyol and sulfate gives a remarkable control of shape[11] and stabilizing agents for instance polyvinylpyrrolidone, PVP, help to control the size.[12] Seed-mediated growth of palladium nanocrystals has been a successful approach to prepare size-controlled nanoparticles,[13] albeit significant achievements have been obtained by the seedless growth of palladium nanocrystals with tunable structures[14] and ultrathin palladium nanosheets.[15] The shape-controlled synthesis of nanoparticles influences the surface coordination chemistry and so the surface properties of palladium nanomaterials.[16] The molecular mechanisms of surface ligands on catalysis and support effects in supported palladium nanocatalysts are linked to the shape and size of nanoparticles.[17,18,19,20] Therefore, performance of palladium nanocatalysts is influenced by their properties at the atomic and molecular level. To take advantage of palladium nanoparticles the next step is the immobilization of them on solid supports as it allows recovery of the catalysts and easier work-up and purification processes.[21] It has found widespread use in various areas of organic synthesis such as carbon-carbon coupling reactions,[22,23] especially in water,[24,25,26] or as recyclable material,[27,28] hydrogenation of oxoderivatives,[29] and electrocatalysis,[1,8] often as bimetallic nanocrystals,[30] ethanol oxidation,[31,32] nitroaryl reduction[33,34] or CO_2 storage.[35] Solid supported palladium nanoparticles are often used in hydrogenation of alkenes[36,37,38] and alkynes,[20,39] the system is highly efficient but suffers from low catalytic selectivity.[40] The stereoselective hydrogenation of internal alkynes to Z alkenes is an important process in the synthesis of pharmaceutical and industrially relevant compounds.[41] From the many reported methods,[42,43] remarkable stereoselectivity is achieved by homogeneously dispersed palladium nanoparticles in DMF[44] and by core–shell nanocomposites of palladium nanoparticles covered with an alkyl sulfoxide network on the surface of SiO_2.[45] Recent reports explore the use of bimetallic palladium nanomaterials[46] or supported nanoparticles of non-precious metals[47] in relation to the Z selectivity[48] or the Z/E interconversion of the obtained olefins.[49,50] Due to the presence of Z-alkenes in many biologically active molecules[51] an ideal conversion of easily available internal alkynes into active Z-alkenes with no alteration of the many functional groups that usually are involved in biological products is much desirable. We want to report now the size-controlled growth of monodisperse polycrystalline palladium nanodendrites on the surface of polymers as a reusable catalyst for the green modification of hormones and drugs bearing internal alkynes into their biologically active counterpart having a Z-alkene with complete regio- and stereoselectivity with respect to many other existent functional groups.

[a] Department of Chemistry, Faculty of Science, University of Burgos, 09001 Burgos, Spain.
[b] Advanced Microscopy Unit, Scientific Park Foundation, I+D Building, Miguel Delibes Campus, University of Valladolid, 47011 Valladolid, Spain.

† Electronic Supplementary Information (ESI) available: Experimental details, characterization data, and additional experiments. See DOI: 10.1039/x0xx00000x

View Article Online
DOI: 10.1039/C8GC01522H

Results and discussion

We have recently developed a new functional polymer capable to be easily coated by gold nanoparticles, uniformly distributed on the surface of the polymers, by simply adding a gold(III) solution in water to the polymer.[52] The polymer supported gold nanoparticles material was used as an efficient portable and reusable catalyst for Suzuki reactions in mixed organic-aqueous solvents. The simplicity of the preparation of the catalyst, with no need of additional ligands for protection, encouraged us to look for new competitive catalysts for green catalysis in the synthesis of fine chemicals by heterogeneous catalysis. With this in mind, we performed a systematic search for appropriate substrates for palladium deposition by preparing a variety of differently composed polymers and checked them for palladium nanoparticles deposition. The polymeric films were prepared by the photochemically initiated radical polymerization[52] of monomers **VP**, **A1**, **A4**, **A2HE**, **M2**, **MEGMA**, **MP**, **A12** and **C**, which was used as cross-linking agent. **DMPA** (1.5% wt) was employed as photochemical initiator (Figure 1). The polymer films were characterized by IR, TGA, UV-Vis, SEM and EDX (See the Supporting Information section).

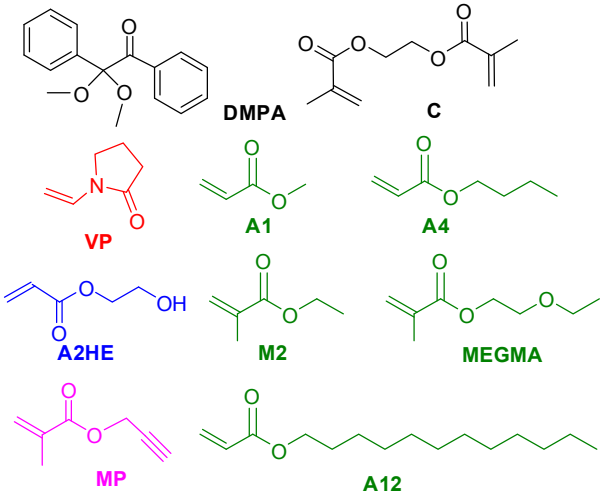

xVP:yMM // zC

xA2HE:yMP // zC

Films (%)	VP	A12	A4	A1	M2	MEGMA	A2HE	MP	C
PBM2	50				50				0
PBMEGMA	50					50			0
PB0	60		40						0
PB20_80A12	20	80							10
PB20_80A4	20		80						10
PB20_80A1	20			80					10
PB0_100A4			100						10
PB0_100A1				100					10
PB80_20A1	80			20					10
PB80_20A4	80		20						10
A2HE5							100		10
JG25_SA2							95	5	10

Figure 1 Monomeric components of the films and photoinitiator (DMPA) and composition of the different polymers; "x", "y" and "z" represent the relations between components; x+y = 100%, z is the percentage respect x+y.

The films (1×1 cm) were submerged in a 5 mM $PdCl_2$/2NaCl solution in water (3 mL) for 20 h in the dark and then washed with water. The polymers bearing acrylate esters and vinylpyrrolidone as components gave rise to deposits of Pd nanoparticles on the surface. **PB20_80A1** gave the best performance under the conditions described for the direct deposit of Pd nanoparticles. Scanning electron microscopy (SEM) showed the surface of the polymer uniformly coated by clusters of homogeneously sized Pd nanoparticles. EDS analysis of the palladium nanoclusters on the surface of the polymer **Pd@PB20_80A1** showed they were only composed by palladium but the XPS analysis showed a proportion of 20:80 for Pd(II):Pd(0) on the surface. The preparation of Pd nanoparticles on film, **Pd@PB20_80A1**, and the transfer to carbon band, **Pd@Cband**, are shown in Figure 2.

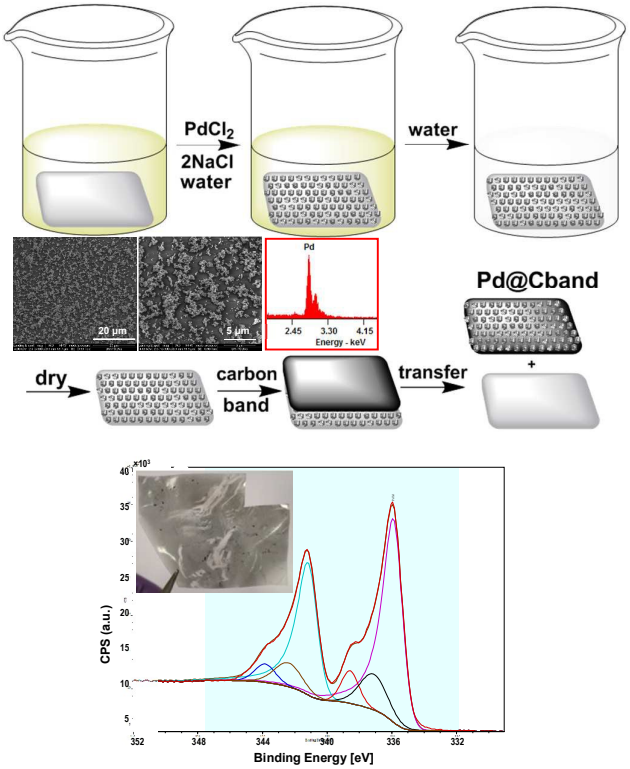

Figure 2 Representative experiments for the preparation of polymer supported palladium nanoparticles **Pd@PB20_80A1** and the dry transfer to carbon band **Pd@Cband**. Inset: Two SEM images of the original covering of the polymer, **Pd@PB20_80A1**, before transfer; left, scale bar 20 µm, center, scale bar 5 µm, right, EDS analysis of the palladium nanoparticles **Pd@PB20_80A1** as an expansion of the region from 2.3 to 4.2 keV scale. Lower: XPS analysis of the palladium nanoclusters on the surface of the polymer **Pd@PB20_80A1** showing a proportion of 20:80 for Pd(II):Pd(0). The covering was homogeneous for several cm^2. Inset: a photograph of the polymer **Pd@PB20_80A1** covered by palladium nanoclusters.

View Article Online
DOI: 10.1039/C8GC01522H

After rinsing in distilled water and drying, the clusters were transferred by simply pressing to a carbon band for high vacuum TEM (Figure 3).

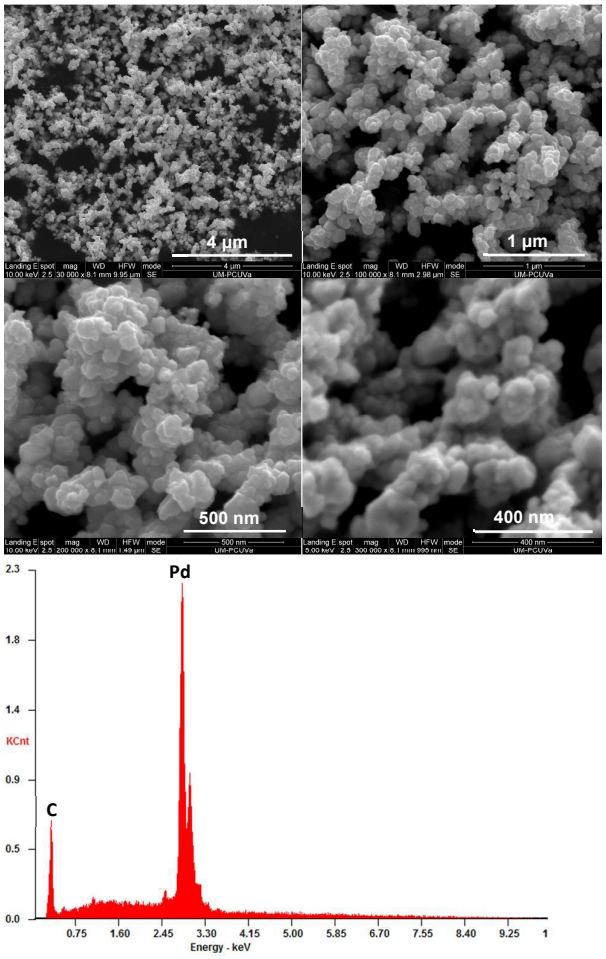

Figure 3 SEM images of palladium nanoclusters on carbon band, **Pd@Cband**, after homogeneous coating of polymer **PB20_80A1** by palladium nanoclusters (5 mM $PdCl_2$/2NaCl solution in 300 µL water for 20 h in the dark) and carbon band transfer, (upper left) scale bar 4 µm, (upper right) scale bar 1 µm, (middle left) scale bar 500 µm, (middle right) scale bar 400 µm. (Lower left) EDS analysis of the palladium nanoclusters transferred on carbon band.

A more detailed view of the palladium nanoparticles was obtained by transmission electron microscopy (TEM) of the palladium nanoparticles dispersed in solution from the deposited sample (Figure 4). All $PdCl_2$ was consumed in the experiment; therefore the Pd nanoparticles appeared as clean discrete individual particles. These Pd nanoparticles were polycrystalline dendrites showing an internal structure with radial growth and an average diameter of 75 nm. The Figure 4, lower left figure, shows the image of a Pd nanoparticle obtained by means of high resolution transmission electron microscopy (HRTEM). The fringes with lattice of 1.95 and 2.23 Å are calculated by measuring the separation of 10 planes and dividing these values by 10. These values can be indexed as {111} and {200} of fcc Pd, respectively.

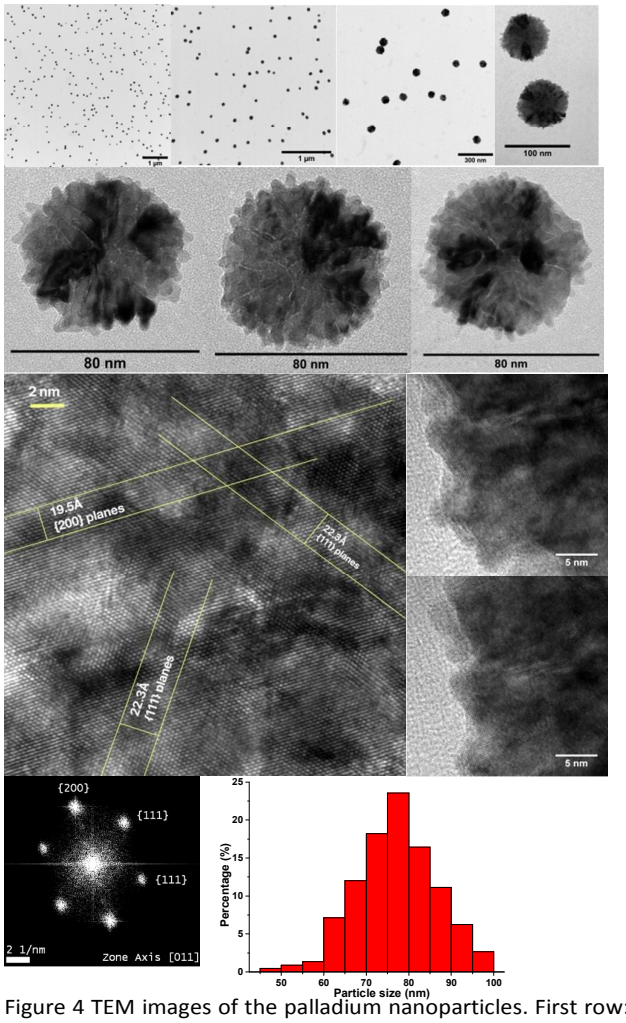

Figure 4 TEM images of the palladium nanoparticles. First row: medium resolution TEM, scale bar 1 µm, 1 µm, 300 nm, 100 nm, 80 nm. Second row: high resolution TEM of individual nanoparticles, scale bar 100 nm. Third row: left: high resolution TEM of an individual nanoparticle, the lattice spacing intervals of 19.5 and 22.3 Å correspond to blocks of 10 planes each and can be indexed as {200} and {111} of fcc Pd, respectively; right: high resolution TEM of individual nanoparticles showing the boundaries of the nanoparticle, scale bar 5 nm. Fourth row: left: FFT of the HRTEM image showing the interplanar distances corresponding to {111} and {222} family planes, a pattern corresponding to a f.c.c. crystal in the zone axis [011]. Right: Distribution of the particle size.[53]

When the film **PB80_20A4** (1×1 cm) was submerged in a 5 mM $PdCl_2$/2NaCl solution in water (3 mL) for 20 h in the dark, there was no initial deposition of Pd nanoparticles but instead, palladium chloride was adsorbed uniformly on the surface of the material. EDS analysis showed there were composed of palladium chloride nanoclusters but XPS analysis of **$PdCl_2$@PB80_20A4** showed a proportion of 45:55 of Pd(II):Pd(0) therefore it was partially reduced in the surface (Figure 5). Hydrogenation for 10 minutes at 5 atm gave rise to size controlled deposition of uniformly distributed palladium

View Article Online
DOI: 10.1039/C8GC01522H

nanoparticles on the surface of the polymer (Figure 6). Similar results were also obtained for **PB80_20A1**, therefore, the results in this case are not so tightly dependent on the acrylate ester as in previous case. To have an idea of the loadings of the polymers, two samples of the polymers with better results (around 8 milligrams each) were weighed before and after reaction with the Pd(II) salt in solution. The increase in weight was around 1.1% for **PB20_80A1** and 2.4% for **PB80_20A4**. In the first case the repeatability was lower. The representative experiments for the preparation of polymer supported Pd nanoparticles **Pd@PB80_20A4** are shown in the Figure 5.

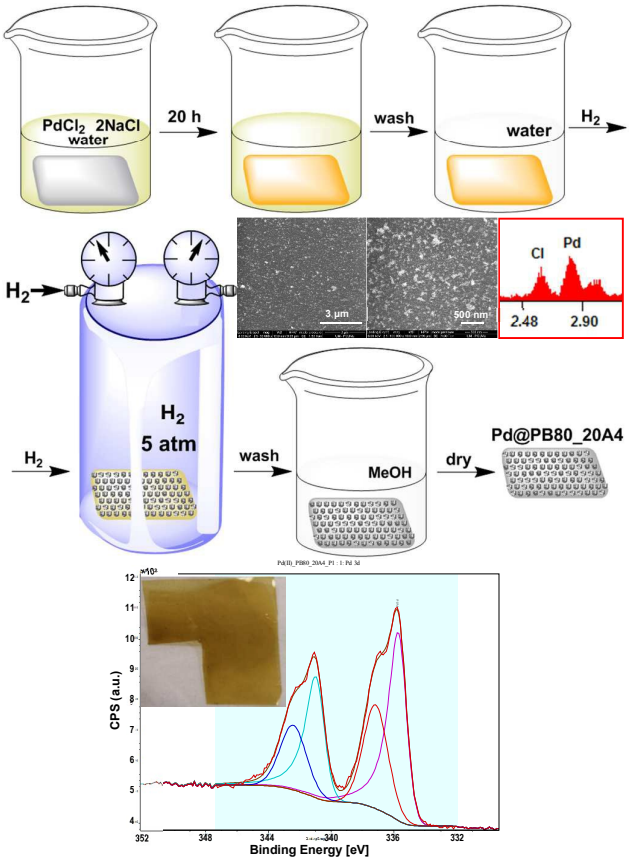

Figure 5 Representative experiments for the preparation of polymer supported Pd nanoparticles **Pd@PB80_20A4**. Inset: Two SEM images of the original covering of the polymer with palladium chloride, left, scale bar 3 µm, center, scale bar 500 nm, right, EDS analysis of the palladium chloride nanoclusters **$PdCl_2$@PB80_20A4** as an expansion of the region from 2.3 to 3.0 keV scale. Lower: XPS analysis of the palladium chloride nanoclusters on the surface of the polymer **Pd@PB80_20A4**. Inset: photograph of the polymer covered by palladium chloride nanoclusters **Pd@PB80_20A4**, the covering is homogeneous for several cm^2.

Hydrogenation of the polymer did not need a solvent, albeit a range of solvents such as methanol or ethanol could be used with similar results. The Pd nanoparticles obtained by reduction on the polymer showed similar size and shape to the previously obtained by direct deposition of the film. The nanoparticles appeared, as in previous case, as polycrystalline dendrites with average diameters of 75 nm, covering the surface of the polymer homogeneously for several cm^2, an ideal situation for their use as supported catalysts. XPS analysis of the reduced **Pd@PB80_20A4** showed a 100% Pd(0) on the surface (Figure 6).

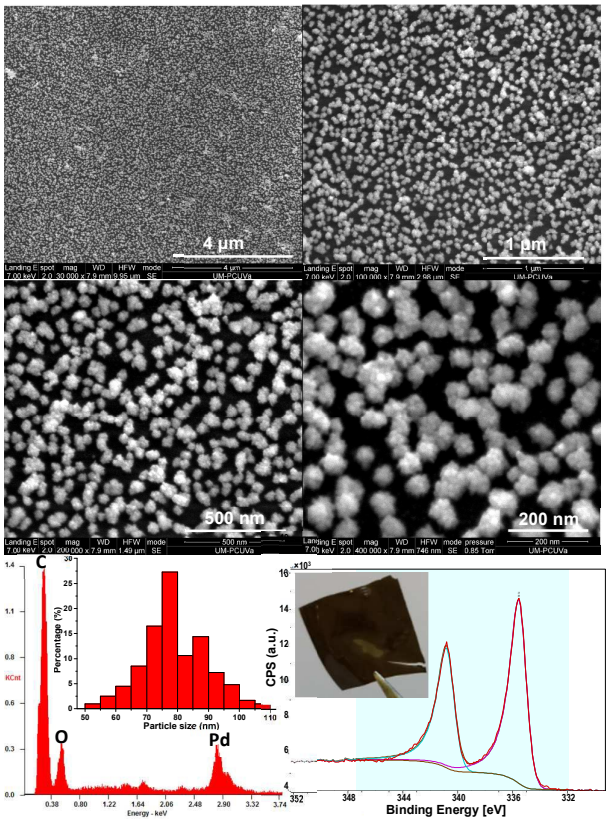

Figure 6 SEM images of palladium nanoparticles on polymer, **Pd@PB80_20A4**, (upper left) scale bar 4 µm, (upper right) scale bar 1 µm, (middle left) scale bar 500 µm, (middle right) scale bar 200 µm (lower left) EDS and (lower right) XPS analysis of the palladium nanoparticles on the surface of the polymer **Pd@PB80_20A4**. Inset: (lower left) distribution of the particle size[53] and (lower right) photograph of the polymer covered by palladium nanoparticles **Pd@PB80_20A4**, the covering is homogeneous for several cm^2.

Dendritic-like palladium nanostructures have been found only use in the preparation of electrodes for electrocatalytic ethanol oxidation,[54-55] formic acid oxidation,[56-57] or lithium–oxygen batteries.[58] We have oriented our efforts to the use of our supported Pd catalyst on the still highly interesting[59] semihydrogenation of disubstituted alkynes with molecular hydrogen. For initial experiments we selected as model compound dimethyl acetylendicarboxylate (DMAD), a typical Michael acceptor with an electron-deficient triple bond whose simplicity in ^1H NMR spectroscopy makes easy following the reaction pathway. We quickly noticed that **Pd@PB20_80A1**, **Pd@PB80_20A4** and **Pd@PB80_20A1** gave the best

View Article Online
DOI: 10.1039/C8GC01522H

performance in the hydrogenation by using very simple conditions. Thus, in 10 mL vials, 500 mg of dimethyl acetylenedicarboxylate were dissolved in 5 ml of methanol or ethanol, a piece of polymer, 0.5×0.5 cm, was added to the solution and the vial was placed in a reactor, then H_2 was introduced to the chamber until reaching 5 atm and the mixture remained under H_2 for 15 hours. After that, excess hydrogen was released, the solid catalyst was removed and the solvent evaporated. The product was checked by ^{1}H NMR as dimethyl maleate (>95% yield) with no traces by ^{1}H NMR of dimethyl fumarate or dimethyl succinate. Leaching of palladium was negligible after analyzing 1mL samples of reaction solutions by ICP mass (less than 2 µM Pd from **Pd@PB20_80A1** reactions and less than 6 µM Pd from **Pd@PB80_20A4/A1** reactions). The catalyst turnover number (TON), defined as product mol/surface, was calculated for **Pd@PB80_20A4** and dimethyl maleate as 0.12 mol×cm^{-2}. The yield was practically the same after recycling **Pd@PB80_20A4** catalyst for six times. The procedure permitted the quantitative transformation of important pharmacological drugs or intermediates for them into related drugs or additional intermediates (Figure 7).

In this way, mifepristone, a steroidal progesterone[60] and glucocorticoid receptor antagonist,[61] used as contraceptive agent and in the treatment of breast cancer,[62] was transformed into aglepristone,[63] a related progesterone antagonist used for the treatment of various progesterone-dependent physiological or pathologic conditions in veterinary medicine. Efavirenz,[64] a non-nucleoside reverse transcriptase inhibitor used as a first-line anti-HIV drug,[65] was transformed into *cis*-dihydroefavirenz,[66] a predicted but yet unavailable efavirenz analogue, thus expanding the pharmaceutical possibilities of fluorine-containing pharmaceuticals.[67] The 8-bromo-7-(2-butyn-1-yl)-3-methylxanthine, a key intermediate for the synthesis of linagliptin,[68] a xanthine dipeptidyl peptidase-4 (DPP-4) inhibitor for the treatment of type 2 diabetes,[69] was transformed into (*Z*)-8-bromo-7-(2-buten-1-yl)-3-methylxanthine, a new intermediate on the way to new DPP-4 inhibitors.[70] The presence of the sensitive bromo substituent in the reduced product constitutes a remarkable proof of the selectivity of the catalytic semihydrogenation selectivity of the described process, albeit in this case a purification step is required. Tazarotene,[71] a receptor selective retinoid that specifically binds to retinoid receptors in the skin after ester hydrolysis,[72] currently used for topical treatment of psoriasis, was then converted into (*Z*)-dihydrotazarotene [ethyl (*Z*)-6-(2-(4,4-dimethylthiochroman-6-yl)vinyl)nicotinate] a new potential retinoid,[73] in good yield. Tazarotene was less reactive under the same reaction conditions, therefore an easy separation from the remaining starting material, that was repeatedly reused, was also needed. In view of the importance of all-(*Z*) polyunsaturated lipids for biological purposes, we selected the available pentacosa-10,12-diynoic acid and subjected the compound to semihydrogenation conditions, from which we obtained a scarce yield of the corresponding (*Z*)(*Z*)-pentacosa-10,12-dienoic acid due to the natural tendency of the starting material to form Langmuir–Blodgett structures that polymerize under the light giving blue and red solutions.[74]

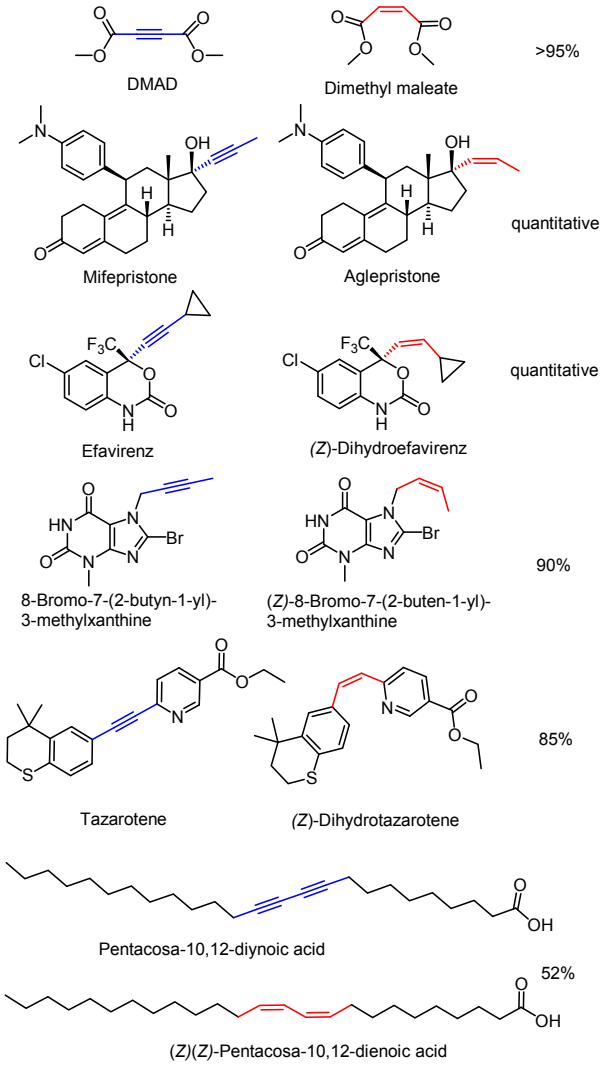

Figure 7 The transformation of pharmacological drugs or intermediates by selective catalytic semihydrogenation. In blue, starting materials reactive moiety, in red, semihydrogenation products modified moiety.

To compare the reported conditions with a common palladium on carbon catalyst, we performed the same reactions in the presence of commercial palladium on carbon, obtaining in all cases mixtures of products coming from different hydrogenation patterns, such as saturated triple bonds, reduction of internal double bonds and dehalogenation products, all coming from the previous starting materials. We also tested the commercial Lindlar catalyst in the same conditions used for the previous experiments, founding as well mixtures of the *Z*-semihydrogenation product with substantial amounts of the doubly hydrogenated triple bond and other by-products. Under ideal conditions for the Lindlar catalyst,[75] tetrahydrofuran as solvent in the presence of quinoline as co-catalyst, the results were more closely related to the obtained with the palladium on polymer catalysts but there was no

View Article Online
DOI: 10.1039/C8GC01522H

more a green process and the recyclability of the catalyst was lost. As a result, the selectivity of the *Z*-semihydrogenation reaction in the presence of the new Pd nanoparticles material was carefully checked and proved to be much superior to common catalysts and comparable to previously reported examples.[76-77]

We were intrigued by the *Z*-semihydrogenation selectivity, for that reason the interactions of the different substrates were simulated using DFT calculations. All calculations were carried out using the quantum chemical software ORCA 4.0.1.2.[78] Pd was described using the relativistic effective-core potentials (LANL2DZ).[79] The basis sets for C, O and H were the Ahlrichs basis def2-SVP.[80] B3LYP[81-82] was selected as an exchange-correlation energy functional. The combination B3LYP/LANL2DZ model chemistry was chosen because it was found reliable for systems formed by organic molecules adsorbed on palladium.[83-84] The geometry of the single-layer Pd lattice was frozen during geometry optimization and frequency calculation. The interaction energies were computed as $\Delta E = E_{sub/Pd10} - (E_{Pd10} + E_{sub})$, with "sub" being the adsorbed substrate. The Cartesian coordinates of the optimized geometries can be found in the Supporting Information. For this simulation, a single layer of 10 atoms of Pd was used (Pd_{10}). A simplified model of mifepristone molecule singly adsorbed by the C≡C bond on the plane sites of the {111} faces interacted by bridge coordination with three Pd atoms of the cluster (Figure 8A). By means of this interaction the carbon–carbon bond distance was 138 pm. To simulate the interaction of the product of hydrogenation through the C=C bond with the Pd layer two possibilities were explored. The difference of these two possibilities was the relative orientation of the added hydrogen atoms with the OH group. In one of them, these two hydrogen atoms were oriented at the opposite side of the OH group (Figure 8B) and in the other possibility these hydrogen atoms were oriented at the same side of the OH group (Figure 8C). We must keep in mind that the free rotation around the C-C single bond HOC-C(H)C is a way of conversion between both structures once the interaction to the metal layer is broken and the steric hindrance reduced. It was observed that in both cases the interaction of the product of hydrogenation with the same plane is slightly different because there was not bridging interaction between the carbon atoms and the Pd atoms. All these facts were in good agreement with reported similar systems.[84]

The difference of the energy of the interaction between the model of the mifepristone with Pd_{10} and alkene substrates with Pd_{10} was estimated. The interaction energies resulted more marked for the mifepristone model than the observed for the product of its hydrogenation by 49.6 kcal/mol for the structure of Figure 7B and by 50.3 kcal/mol for the structure of Figure 7C. The higher stabilization found for the mifepristone model is in good agreement with a higher affinity of the C≡C bond than the C=C bond for the adsorption of the mifepristone. This higher affinity is related with the experimentally observed semihydrogenation of the mifepristone when compared with the lack of reduction of the semihydrogenation product.

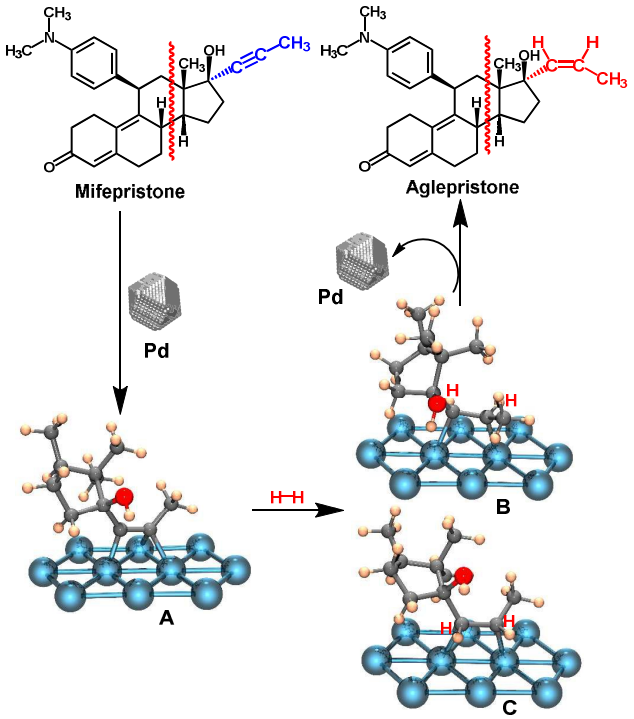

Figure 8 A sketch showing the interaction with a layer of ten atoms of palladium corresponding to a plane {111} of the simplified model of mifepristone (A), the product of hydrogenation at the opposite side of the OH group (B) and the product of hydrogenation at the same side to the OH group (C) that after disconnection give rise to aglepristone.

Therefore, the remarkable selectivity and the simplicity of the preparation of the catalyst in water, with no need of additional ligands for stabilization, make the system competitive to known solid supported Pd nanoparticles catalysts for the semihydrogenation reaction in green solvents.[85] The polymer supported Pd nanoparticles material can be very useful for heterogeneous catalysis in the synthesis of important drugs, or intermediates for drugs, in a highly sustainable chemistry, because of the reusability of catalyst and alcohol solvent with no leaching of palladium into the reaction mixture.

Conclusions

In conclusion, we have described the preparation of new monodisperse polycrystalline palladium nanoparticles uniformly distributed on the surface of polymers, by simply adding a palladium(II) solution in water to the polymers. The polymer supported palladium nanoparticles materials were used as efficient portable and reusable catalysts for the stereoselective semihydrogenation reactions of important internal alkynes to (*Z*)-alkenes in green solvents.

View Article Online
DOI: 10.1039/C8GC01522H

Experimental section

Experimental details for all materials are described in the Supporting Information. They can be followed in figures S1-S4 and the accompanying text, characterization data for the functional polymers can be followed in figures S5-S13. The results of catalysis for reduction of DMAD can be followed in figures S14-S16 and the accompanying text. Reduction of materials with pharmacological interest and characterization of reduced materials can be followed in figures S17-S52. Cartesian coordinates from DFT calculations can be followed in tables S1-S3.

Acknowledgements

We gratefully acknowledge financial support from the Ministerio de Economía y Competitividad, Spain, and Fondo Europeo de Desarrollo Regional (FEDER) (Projects CTQ2015-71353-R and MAT2014-54137-R) and Junta de Castilla y León, Consejería de Educación y Cultura y Fondo Social Europeo (Projects BU051U16 and BU061U16). This research has made use of the high performance computing resources of the Castilla y León Supercomputing Center (SCAYLE, www.scayle.es), financed by the European Regional Development Fund (ERDF). J.G.-C. thanks Ministerio de Economía y Competitividad for his predoctoral FPU fellowship. This paper is dedicated to the memory of the late Dr. Stefano Marcaccini.

References

1 A. Chen and C. Ostrom, *Chem. Rev*., 2015, **115**, 11999−12044.
2 Y. Xia, Y. Xiong, B. Lim and S. E. Skrabalak, *Angew. Chem. Int. Ed*., 2009, **48**, 60–103.
3 B. Lim, M. Jiang, J. Tao, P. H. C. Camargo, Y. Zhu and Y. Xia, *Adv. Funct. Mater*., 2009, **19**, 189–200.
4 Y. Wang, H.-C. Peng, J. Liu, C. Z. Huang and Y. Xia, *Nano Lett*., 2015, **15**, 1445−1450.
5 J. Watt, S. Cheong, M. F. Toney, B. Ingham, J. Cookson, P. T. Bishop and R. D. Tilley, *ACS Nano*, 2010, **4**, 396–402.
6 S. Corra, U. Lewandowska, E. M. Benetti and H. Wennemers, *Angew. Chem. Int. Ed*., 2016, **55**, 8542 –8545.
7 Y. Li, Y. Yan, Y. Li, H. Zhang, D. Li and D. Yang, *CrystEngComm*, 2015, **17**, 1833–1838.
8 Y. Zhang, X. Zhu, J. Guo and X. Huang, *ACS Appl. Mater. Interfaces,* 2016, **8**, 20642−20649.
9 X. Yin, J. Wu, P. Li, M. Shi and H. Yang, *ChemNanoMat,* 2016, **2**, 37–41.
10 C. Shang, W. Hong, Y. Guo, J. Wang and E. Wang, *Chem. Eur. J.,* 2017, **23**, 5799–5803.
11 H. Huang, Y. Wang, A. Ruditskiy, H.-C. Peng, X. Zhao, L. Zhang, J. Liu, Z. Ye and Y. Xia, *ACS Nano,* 2014, **8**, 7041–7050.
12 C. Evangelisti, N. Panziera, A. D'Alessio, L. Bertinetti, M. Botavina and G. Vitulli, *J. Catal.,* 2010, **272**, 246–252.
13 Y. Xia, K. D. Gilroy, H.-C. Peng and X. Xia, *Angew. Chem. Int. Ed.,* 2017, **56**, 60–95.
14 Y. Zhang, M. Wang, E. Zhu, Y. Zheng, Y. Huang and X. Huang, *Nano Lett.,* 2015, **15**, 7519−7525.
15 X. Yin, X. Liu, Y.-T. Pan, K. A. Walsh and H. Yang, *Nano Lett.,* 2014, **14**, 7188−7194.
16 P. Liu, R. Qin, G. Fu and N. Zheng, *J. Am. Chem. Soc*., 2017, **139**, 2122−2131.
17 P. Liu, Y. Zhao, R. Qin, S. Mo, G. Chen, L. Gu, D. M. Chevrier, P. Zhang, Q. Guo, D. Zang, B. Wu, G. Fu and N. Zheng, *Science,* 2016, **352**, 797-801.
18 K. Kim, Y. Jung, S. Lee, M. Kim, D. Shin, H. Byun, S. J. Cho, H. Song and H. Kim, *Angew. Chem. Int. Ed.,* 2017, **56**, 6952–6956.
19 G. M. Lari, B. Puértolas, M. Shahrokhi, N. López and J. Pérez-Ramírez, *Angew. Chem. Int. Ed.,* 2017, **56**, 1775–1779.
20 G. Vilé, N. Almora-Barrios, S. Mitchell, N. López and J. Pérez-Ramírez, *Chem. Eur. J.,* 2014, **20**, 5926–5937.
21 D. Astruc, F. Lu and J. R. Aranzaes, *Angew. Chem. Int. Ed.,* 2005, **44**, 7852–7872.
22 A. Fihri, M. Bouhrara, B. Nekoueishahraki, J.-M. Basset and V. Polshettiwar, *Chem. Soc. Rev.,* 2011, **40**, 5181–5203.
23 A. Biffis, P. Centomo, A. Del Zotto and M. Zecca, *Chem. Rev.,* 2018, **118**, 2249−2295.
24 G. Yun, Z. Hassan, J. Lee, J. Kim, N.-S. Lee, N. H. Kim, K. Baek, I. Hwang, C. G. Park and K. Kim, *Angew. Chem. Int. Ed.,* 2014, **53**, 6414–6418.
25 T. Nishikata, H. Tsutsumi, L. Gao, K. Kojima, K. Chikama and H. Nagashima, *Adv. Synth. Catal.,* 2014, **356**, 951–960.
26 S. Ogasawara and S. Kato, *J. Am. Chem. Soc.,* 2010, **132**, 4608–4613.
27 E. Hariprasad and T. P. Radhakrishnan, *ACS Catal.,* 2012, **2**, 1179−1186.
28 P. Pachfule, M. K. Panda, S. Kandambeth, S. M. Shivaprasad, D. D. Díaz and R. Banerjee, *J. Mater. Chem. A,* 2014, **2**, 7944–7952.
29 A. Balouch, A. A. Umar, A. A. Shah, M. M. Salleh and M. Oyama, *ACS Appl. Mater. Interfaces,* 2013, **5**, 9843−9849.
30 K. D. Gilroy, A. Ruditskiy, H.-C. Peng, D. Qin and Y. Xia, *Chem. Rev.,* 2016, **116**, 10414−10472.
31 L. Ren, L. Yang, P. Yu, Y. Wang and L. Mao, *ACS Appl. Mater. Interfaces,* 2013, **5**, 11471−11478
32 R. Yue, H. Wang, D. Bin, J. Xu, Y. Du, W. Lu and J. Guod, *J. Mater. Chem. A,* 2015, **3**, 1077–1088.
33 E. D. Sultanova, V. V. Salnikov, R. K. Mukhitova, Y. F. Zuev, Y. N. Osin, L. Y. Zakharova, A. Y. Ziganshina and A. I. Konovalov, *Chem. Commun.,* 2015, **51**, 13317—13320.
34 Y.-M. Lu, H.-Z. Zhu, W.-G. Li, B. Hu and S.-H. Yu, *J. Mater. Chem. A,* 2013, **1**, 3783–3788.
35 A. Modak, M. Pramanik, S. Inagakib and A. Bhaumik, *J. Mater. Chem. A,* 2014, **2**, 11642–11650.
36 S. K. Mahato, R. U. Islam, C. Acharya, M. J. Witcomb and K. Mallick, *ChemCatChem,* 2014, **6**, 1419–1426.
37 M. Iwanow, J. Finkelmeyer, A. Söldner, M. Kaiser, T. Gärtner, V. Sieber and B. König, *Chem. Eur. J.,* 2017, **23**, 12467–12470.
38 S. K. Surmiak, C. Doerenkamp, P. Selter, M. Peterlechner, A. H. Schäfer, H. Eckert and A. Studer, *Chem. Eur. J.,* 2017, **23**, 6019–6028.
39 Y. Gao, C.-A. Chen, H.-M. Gau, J. A. Bailey, E. Akhadov, D. Williams and H.-L. Wang, *Chem. Mater.,* 2008, **20**, 2839–2844.
40 A. S. Reddy and K. C. K. Swamy, *Angew. Chem. Int. Ed.,* 2017, **56**, 6984–6988.
41 K. Chernichenko, A. Madarász, I. Pápai, M. Nieger, M. Leskelä and T. Repo, *Nat. Chem.,* 2013, **5**, 718-723.
42 M. Crespo-Quesada, F. Cárdenas-Lizana, A.-L. Dessimoz and L. Kiwi-Minsker, *ACS Catal.,* 2012, **2**, 1773−1786.
43 J. Lei, L. Su, K. Zeng, T. Chen, R. Qiu, Y. Zhou, C.-T. Au and S.-F. Yin, *Chem. Eng. Sci.,* 2017, **171**, 404–425.
44 J. Hori, K. Murata, T. Sugai, H. Shinohara, R. Noyori, N. Arai, N. Kurono and T. Ohkuma, *Adv. Synth. Catal.,* 2009, **351**, 3143–3149.

View Article Online
DOI: 10.1039/C8GC01522H

45 T. Mitsudome, Y. Takahashi, S. Ichikawa, T. Mizugaki, K. Jitsukawa and K. Kaneda, *Angew. Chem. Int. Ed.,* 2013, **52**, 1481–1485.
46 J. Liu, Y. Zhu, C. Liu, X. Wang, C. Cao and W. Song, *ChemCatChem,* 2017, **9**, 4053–4057.
47 F. Chen, C. Kreyenschulte, J. Radnik, H. Lund, A.-E. Surkus, K. Junge and M. Beller, *ACS Catal.,* 2017, **7**, 1526−1532.
48 F. Zaera, *ACS Catal.,* 2017, **7**, 4947−4967.
49 S. Furukawa and T. Komatsu, *ACS Catal.,* 2016, **6**, 2121−2125.
50 K. Tokmic and A. R. Fout, *J. Am. Chem. Soc.,* 2016, **138**, 13700−13705.
51 S. J. Meek, R. V. O'Brien, J. Llaveria, R. R. Schrock and A. H. Hoveyda, *Nature,* 2011, **471**, 461-466.
52 J. García-Calvo, V. García-Calvo, S. Vallejos, F. C. García, M. Avella, J.-M. García and T. Torroba, *ACS Appl. Mater. Interfaces,* 2016, **8**, 24999–25004.
53 C. A. Schneider, W. S. Rasband and K. W. Eliceiri, *Nat. Methods,* 2012, **9**, 671-675.
54 K. Qi, Q. Wang, W. Zheng, W. Zhang and X. Cui, *Nanoscale,* 2014, **6**, 15090–15097.
55 S. J. Ye, D. Y. Kim, S. W. Kang, K. W. Choi, S. W. Han and O. O. Park, *Nanoscale,* 2014, **6**, 4182–4187.
56 A. Klinkova, P. D. Luna, E. H. Sargent, E. Kumacheva and P. V. Cherepanov, *J. Mater. Chem. A,* 2017, **5**, 11582–11585.
57 T. Huang, S. K. Moon and J.-M. Lee, *Sustainable Energy Fuels* 2017, **1**, 450–457.
58 S. J. Ye, D. Y. Kim, D. W. Kim, O. O. Park and Y. Kang, *J. Mater. Chem. A,* 2016, **4**, 578–586.
59 D. B. Burueva, K. V. Kovtunov, A. V. Bukhtiyarov, D. A. Barskiy, I. P. Prosvirin, I. S. Mashkovsky, G. N. Baeva, V. I. Bukhtiyarov, A. Y. Stakheev and I. V. Koptyug, *Chem. Eur. J.,* 2018, **24**, 2547–2553.
60 A. Yamada, Y. Kazui, H. Yoshioka, A. Tanatani, S. Mori, H. Kagechika, S. Fujii, *ACS Med. Chem. Lett.,* 2016, **7**, 1028−1033.
61 C. A. Sanhueza, M. M. Baksh, B. Thuma, M. D. Roy, S. Dutta, C. Préville, B. A. Chrunyk, K. Beaumont, R. Dullea, M. Ammirati, S. Liu, D. Gebhard, J. E. Finley, C. T. Salatto, A. King-Ahmad, I. Stock, K. Atkinson, B. Reidich, W. Lin, R. Kumar, M. Tu, E. Menhaji-Klotz, D. A. Price, S. Liras, M. G. Finn and V. Mascitti, *J. Am. Chem. Soc.,* 2017, **139**, 3528−3536.
62 Y. Lin, R. Liu, P. Zhao, J. Ye, Z. Zheng, J. Huang, Y. Zhang, Y. Gao, H. Chen, S. Liu, J. Zhou, C. Chen and H. Chen, *Eur. J. Med. Chem.,* 2018, **146**, 354-367.
63 A. Gogny and F. Fiéni, *Theriogenology,* 2016, **85**, 555–566.
64 S. Li and J.-A. Ma, *Chem. Soc. Rev.,* 2015, **44**, 7439–7448.
65 M. M. Bastos, C. C. P. Costa, T. C. Bezerra, F. de C. da Silva and N. Boechat, *Eur. J. Med. Chem.,* 2016, **108**, 455-465.
66 D. D. Christ, A. J. Cocuzza, S. S. Ko, J. A. Markwalder, A. E. Mutlib, R. L. Parsons, Jr., M. Patel and S. P. Seitz, *U.S. patent,* 1999, **US 5874430 A 19990223**.
67 Y. Zhou, J. Wang, Z. Gu, S. Wang, W. Zhu, J. L. Aceña, V. A. Soloshonok, K. Izawa and H. Liu, *Chem. Rev.,* 2016, **116**, 422−518.
68 M. Eckhardt, T. Klein, H. Nar and S. Thiemann, in: J. Fischer and D. P. Rotella, Eds., Successful Drug Discovery, *Wiley-VCH Verlag*, 2015, **Ch. 7**, 129-156.
69 W.-L. Wu, J. Hao, M. Domalski, D. A. Burnett, D. Pissarnitski, Z. Zhao, A. Stamford, G. Scapin, Y.-D. Gao, A. Soriano, T. M. Kelly, Z. Yao, M. A. Powles, S. Chen, H. Mei and J. Hwa, *ACS Med. Chem. Lett.,* 2016, **7**, 498−501.
70 L. Juillerat-Jeanneret, *J. Med. Chem.,* 2014, **57**, 2197−2212.
71 I. S. Makarov, C. E. Brocklehurst, K. Karaghiosoff, G. Koch and P. Knochel, *Angew. Chem. Int. Ed.,* 2017, **56**, 12774–12777.
72 A. M. Mansour, *Polyhedron,* 2016, **109**, 99–106.
73 R. Alvarez, B. Vaz, H. Gronemeyer, A. R. de Lera, *Chem. Rev.,* 2014, **114**, 1−125.
74 S. Balakrishnan, S. Lee. and J.-M. Kim, *J. Mater. Chem.,* 2010, **20**, 2302–2304.
75 S. Furukawa and T. Komatsu, *ACS Catal.,* 2016, **6**, 2121−2125.
76 T. Mitsudome, T. Urayama, K. Yamazaki, Y. Maehara, J. Yamasaki, K. Gohara, Z. Maeno, T. Mizugaki, K. Jitsukawa and K. Kaneda, *ACS Catal.,* 2016, **6**, 666−670.
77 T. Mitsudome, M. Yamamoto, Z. Maeno, T. Mizugaki, K. Jitsukawa and K. Kaneda, *J. Am. Chem. Soc.,* 2015, **137**, 13452−13455.
78 N. Frank, The ORCA program system, *WIREs Comput. Mol. Sci.,* 2012, **2**, 73-78. doi: 10.1002/wcms.81.
79 P. Hay and W. Wadt, *J. Chem. Phys*., 1985, **82**, 299-310.
80 F. Weigend and Ahlrichs, *Phys. Chem. Chem. Phys*., 2005, **7**, 3297-3305.
81 A. Becke, *J. Chem. Phys*., 1993, **98**, 5648-5652.
82 C. Lee, W. Yang and R. Parr, *Phys. Rev. B,* 1988, **37**, 785-789.
83 S. Omar, J. Palomar, L. M. Gómez, M. A. Álvarez-Montero and J. J. Rodriguez, *J. Phys. Chem. C,* 2011, **115**, 14180−14192.
84 A. Prestianni, M. Crespo-Quesada, R. Cortese, F. Ferrante, L. Kiwi-Minsker and D. Duca, *J. Phys. Chem. C,* 2014, **118**, 3119−3128.
85 C. Capello, U. Fischer and K. Hungerbühler, *Green Chem.,* 2007, **9**, 927–934.

View Article Online
DOI: 10.1039/C8GC01522H

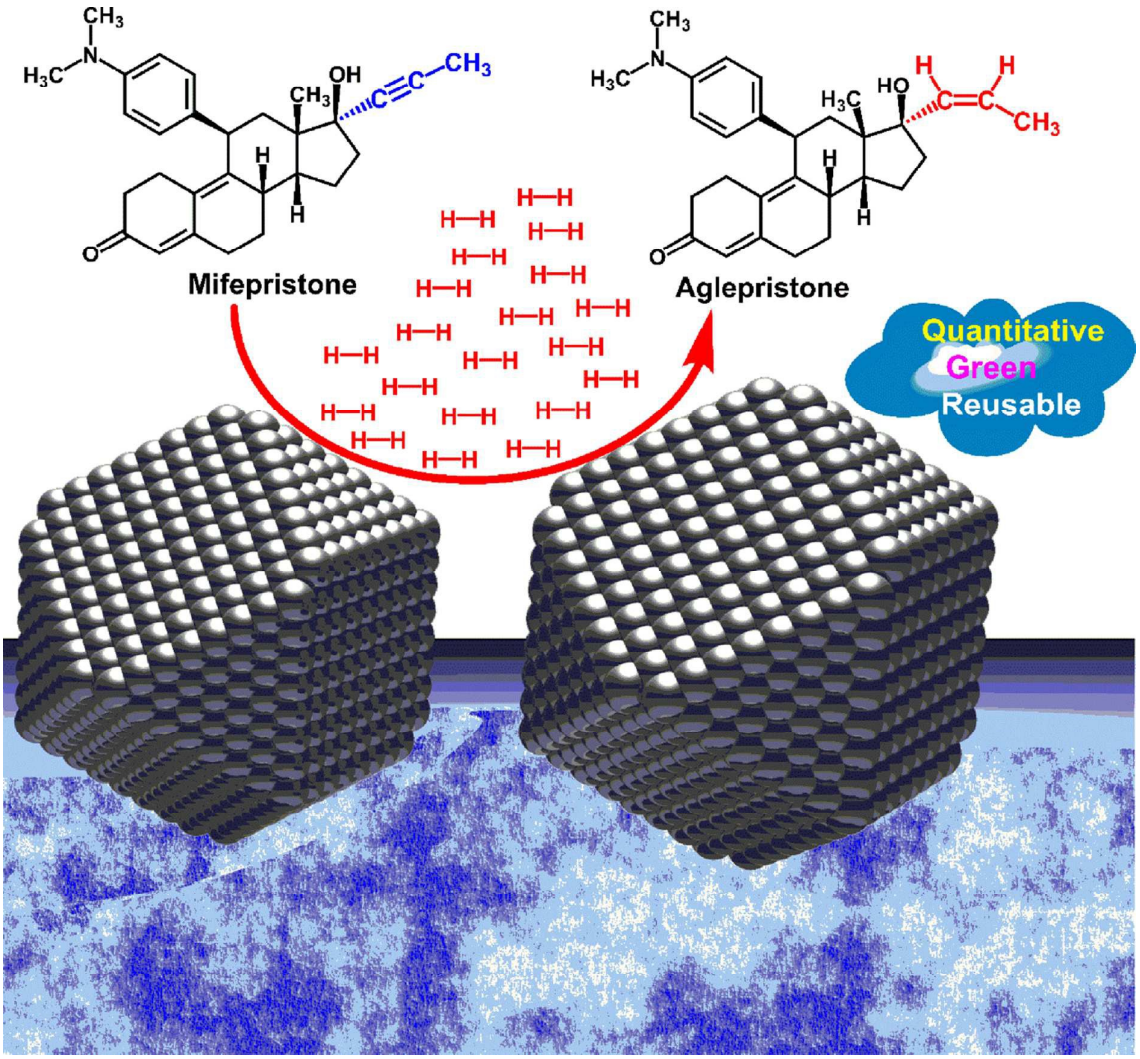

A polymer-supported palladium nanoparticle material catalyzes the stereoselective semihydrogenation of internal alkynes to (Z)-alkenes.